Astronomy & Astrophysics manuscript no. ztf-simulations
March 26, 2016

ZTF anisotropy simulations

U. Feindt[1], A. Goobar[1], M. Kowalski[2], J. Nordin[2], M. Rigault[2]

[1] The Oskar Klein Centre, Physics Department, Stockholm University, Albanova University Center, SE 106 91 Stockholm, Sweden
[2] Institut für Physik, Humboldt-Universität zu Berlin, Newtonstraße 15, 12489 Berlin, Germany

Preprint online version: March 26, 2016

ABSTRACT

Context. [TODO: add?]
Aims. [TODO: add]
Methods. [TODO: add]
Results. [TODO: add]
Conclusions. [TODO: add?]

Key words. cosmology: observations – cosmological parameters – large scale structure of the Universe – supernovae: general

1. Introduction

[TODO: Write me!]

2. Peculiar velocity tidal field

When using SNe Ia (or any other standard candle) to measure peculiar velocities, the deviation from Hubble expansion is interpreted as the effect of the peculiar motion, which mostly affects the redshift of the SN but also its luminosity due to relativistic boosts. The effect of a velocity dipole on the measured luminosity distance can be approximated by a linear term (Bonvin et al. 2006):

$$\begin{aligned}\tilde{d}_{\rm L}(z) &= d_{\rm L}(z) + d_{\rm L}^{(1)}(z,l,b)\\ &= d_{\rm L}(z) + \frac{(1+z)^2}{H(z)}\boldsymbol{n}\cdot\boldsymbol{v}_{\rm d},\end{aligned} \tag{1}$$

where $\boldsymbol{v}_{\rm d}$ is the dipole velocity (bulk flow) vector and $d_{\rm L}$ is the unperturbed luminosity distance calculated by integrating the Hubble law:

$$d_{\rm L}(z) = c(1+z)\int_0^z \frac{{\rm d}z'}{H(z')}. \tag{2}$$

While the velocity of each single SN cannot be constrained well due to the size of the individual uncertainties, the large-scale peculiar velocity field can be reconstructed for a sufficiently large dataset. This can be achieved by minimizing the following χ^2-statistic:

$$\chi^2 = \sum_i \frac{\left|\mu_i - 5\log_{10}\left(\left(d_{\rm L}(z_i) - d_L^{(1)}(z_i,l_i,b_i,\boldsymbol{v}_d)\right)/10\,{\rm pc}\right)\right|^2}{\sigma_i^2}, \tag{3}$$

where the index i denotes the i-th SN of the dataset. $\mu_i = 5\log\left(d_{\rm L}/(10\,{\rm pc})\right)$ is the distance modulus of an SN while σ_i is its uncertainty.

As noted above, the simplest model for a velocity field is a constant bulk flow, i.e. the coherent motion of galaxies in the same direction at the same speed. While such a dipole motion is expected on small scales, finding it on large scales would challenge our understanding of ΛCDM structure formation, which predicts the coherent motion to decrease with the size of the volume, over which it is averaged. The bulk flow is expected to be reciprocal to the distance, with an amplitude of $\lesssim 250\,{\rm km\,s^{-1}}$ at $d = 100\,h^{-1}$ Mpc (see e.g. Kashlinsky et al. 2010). Since only the radial component of the velocity contributes to the effect on the luminosity distances, the bulk flow can be expressed as its amplitude $v_{\rm d}$ and its direction. The velocity term them becomes:

$$\boldsymbol{v}\cdot\boldsymbol{n} = v_{\rm d}\cos(\Delta\theta), \tag{4}$$

where $\Delta\theta$ is the angular separation of the SN and the bulk flow direction.

The next order of perturbation of the luminosity distance in the local universe is a linear distance-dependent velocity term[1], i.e. the multiplication of a tensor by a the position vector $\boldsymbol{x}$. This tensor Σ is defined to be symmetric (i.e. irrotational) and traceless wheres the trace is separated to a scalar term $\tilde{H}$:

$$\boldsymbol{v}(\boldsymbol{x}) = \boldsymbol{v}_{\rm d} + (\tilde{H} + \Sigma)\cdot\boldsymbol{x}. \tag{5}$$

The scalar $\tilde{H}$ is also referred to the *monopole* because it corresponds to a local change in the Hubble law. The traceless tensor, on the other hand, if referred as the *shear*. As it can be derived as a Taylor expansion of the true velocity field, this model is also known the tidal field. It traces the influence of a mass concentration outside the volume, in which the SNe were observed. The distance to this mass can be estimated from the ratio of the bulk flow to the trace in its direction, i.e. by the “convergence” of the velocity field (see e.g. Kaiser 1991; Hoffman et al. 2001)

3. Simulated datasets

To simulate future surveys, supernova redshifts are drawn from a distribution based on a constant volumetric supernova rate that

[1] The constant bulk flow can be thought of as the 0th order of the Taylor expansion of the velocity field. In this case a 3×3 tensor is the first order.

extends the redshift $z = 0.08$. All SNe out to that redshift are expected are above the expected detection threshold [TODO: better wording, what is our detection threashold?]. We restrict the simulations to a specified number of SNe. There the value of the volumetric rate has of no consequence to the simulation. For the distribution of the directions, uniform distributions were used in right ascension α and the sine of the declinations $\sin(\delta)$, which leads to a uniform distribution on the sky. For the main simulation case 1800 coordinates were drawn, for which the declinations were limited to $-20° < \delta < 90°$. Furthermore a zone of avoidance of 10° around the Milky Way, i.e. $-10° < b < 10°$, was excluded by redrawing coordinates in that region. In addition two larger simulation cases were run to assess the possible bias due to the uneven distribution of coordinates in a survey of the northern sky. In the first of these cases, 600 SNe on the southern sky ($\delta < 20°$) were added to the 1800 ZTF SNe, corresponding to SN Ia data from southern surveys such as Skymapper [TODO: add ref]. The other additional case simulated 2400 ZTF SNe in order to disentangle the benefit of southern SNe compared to an increase in statistics on the northern sky. In all cases the coordinates are drawn once and reused for each simulation. [TODO: I could rerun them with redrawing the coordinates every time, though.]

The next step consists in calculating the luminosity distances, d_L, for a redshift, z, and applying a perturbation corresponding to a peculiar velocity field, $\boldsymbol{v}(z, l, b)$, according to eq. (1). We chose to use a simple velocity field with known dipole and shear components that are constant in the whole simulated volume. Using this field we can directly see whether the data distribution leads to a bias in the bulk flow and shear estimates.

The dipole velocity is set to a constant values of $300\,\mathrm{km\,s^{-1}}$ towards $l = 300°, b = 30°$. This corresponds to the bulk flow observed at low redshifts. This shear is expressed as a symmetric, traceless tensor, for which the largest eigenvalue λ_1 is set to $1.5\,\mathrm{km\,s^{-1}\,Mpc^{-1}}$ [TODO: Cite a paper measuring the shear.] with the corresponding eigenvector pointing in the same direction as the bulk flow. The other two eigenvalues are set to $\lambda_2 = \lambda_3 = -\lambda_1/2$ to ensure that the trace is zero. Using the interpretation of the shear as in e.g. Kaiser (1991) or Hoffman et al. (2001), i.e. that the characteristic distance to the main attractor can be estimated by two times the ratio of the bulk flow amplitude and the shear, this velocity field corresponds to the tidal field caused by a mass concentration at a distance of 400 Mpc, a distance slightly beyond that of the Sloan Great Wall. Note that a constant bulk flow and shear of this size over such large scales is not expected within ΛCDM structure. Therefore this case is only used to determine how well the input parameters are reconstructed. [TODO: Rephrase?]

The thus determined distance moduli are then perturbed by a random value drawn from a Gaussian distribution with the a dispersion corresponding to their uncertainties and an additional intrinsic dispersion of 0.1 mag. For simplicity, all uncertainties are fixed to similar values. They were drawn from a Gaussian distribution with mean $\mu = 0.1$ mag and dispersion $\sigma = 0.02$ mag. To prevent too low uncertainties, values less than 0.03 mag were redrawn. Note that this dispersion is smaller than the uncertainties of some literature SNe, especially in older samples, but will on average still give a good estimate for the overall uncertainties.

Once the full dataset has been generated, the analysis methods described in section 2 can be applied to it. This is done by first fitting the Hubble constant while assuming a flat ΛCDM universe with $\Omega_m = 0.3$ to determine the intrinsic scatter of the simulated data set. After that the shear velocity model is fit to subsamples of the data selected by an upper redshift boundary (hereafter referred to as "spheres") or a narrow redshift bins (or "shells").

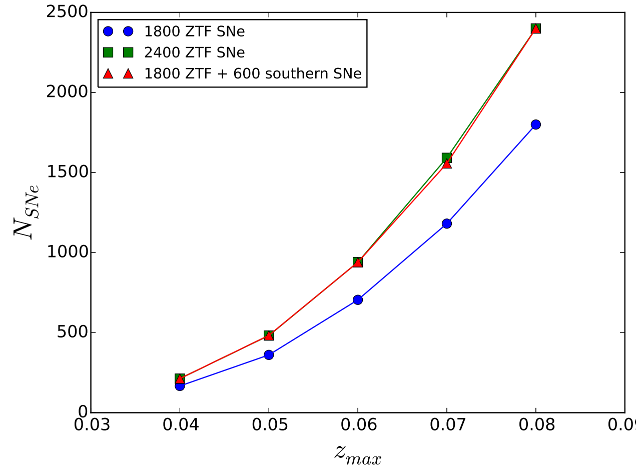

Fig. 1. Median number of simulated SNe with redshift up to z_{max} for simulations of 1800 and 2400 total SNe randomly drawn based on a constant volumetric supernova rate.

4. Results

4.1. Sphere fits [working title]

We analysed the simulated by first fitting the dipole model and then the full tidal field (dipole and shear) to 1000 realizations of the simulation described above. The simulated data were binned in "spheres" with upper redshift cut-offs z_{max} varying between 0.04 and 0.08 to study the evolution of the constraints with depth and statistics. Fig. 1 shows the median number of SNe up to the chosen z_{max} for simulations of 1800 and 2400 total SNe. Note that the redshifts for both simulations of 2400 SNe were drawn separately, leading to slightly different redshift distribution.

Figs. 2–9[2] show the results of the simulations with a constant bulk flow and shear. The most interesting values are the dipole velocity amplitude v_d (Fig. 2 for the dipole fit and Fig. 4 for the tidal field fit), the deviation of the reconstructed dipole direction from the input (Figs. 3 and 5), the shear eigenvalues (Fig. 6), the alignment of the first eigenvector with the simulation input and with the estimated bulk flow direction (Fig. 7) as well the monopole term $\tilde{H}$ (Fig. 8). Recall that the input parameters for the simulation corresponded to $v_d = 300\,\mathrm{km\,s^{-1}}$, $\tilde{\Sigma} = 1.5\,\mathrm{km\,s^{-1}\,Mpc^{-1}}$, and $\tilde{H} = 0$.

Since the dipole velocity amplitude and direction have been estimated with two methods, one of which is an extension of the other, we can investigate how the inclusion of additional fit parameters affects the constraints. The right panel of Fig. 2 shows the uncertainties of the dipole amplitude v_d when only fitting a dipole model. Even for the smallest selected sphere, which contains a few hundred [TODO: specify better] SNe, the uncertainties will be constrained to $\sim 100\,\mathrm{km\,s^{-1}}$. This is comparable to previous studies (e.g. Feindt et al. 2013) and expected since the SNe datasets at this distance already contain a similar number of SNe. The simulations with 2400 SNe constrain v_d similarly well and for both cases the improvement compared to 1800 is compatible with the expectation of a ∼ 13% improvement based on

[2] [TODO: Make sure they are actually ordered correctly 2 3 4 5 6 7 8 9]

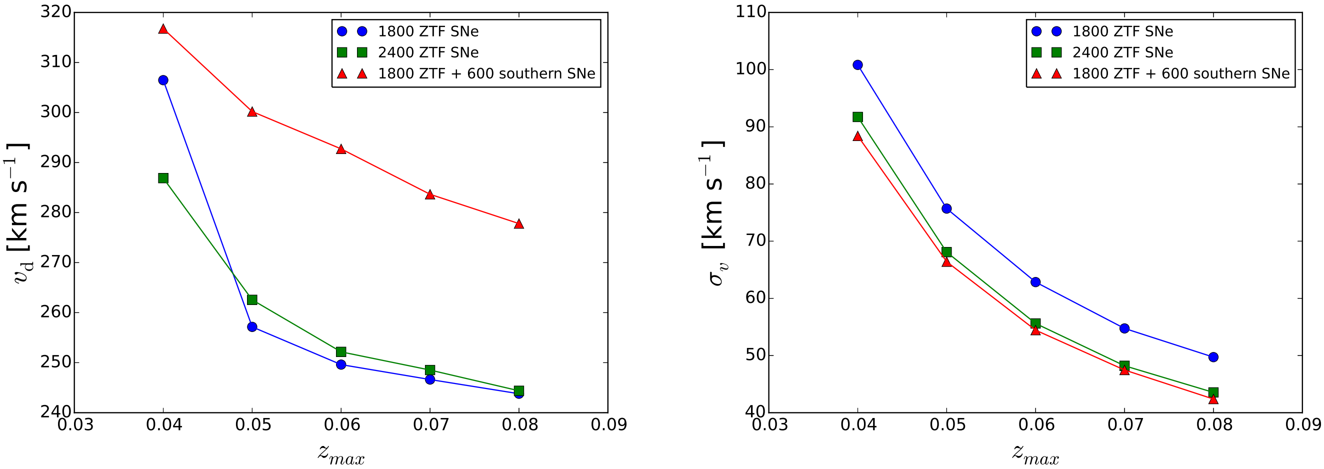

Fig. 2. Results for a bulk flow fit to 1000 random realizations of the simulated data. The left panel shows the median of the reconstructed dipole velocity amplitude $v_{\rm d}$ as a function of the upper redshift cut-off z_{max} while the right panel shows its median uncertainty.

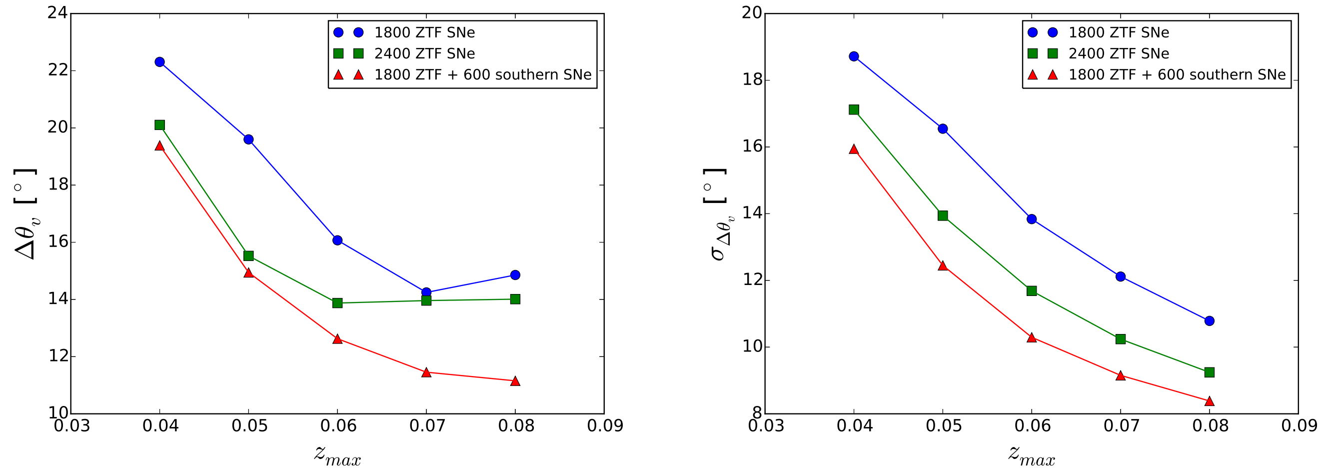

Fig. 3. Results for a bulk flow fit as in Fig. 2. The left panel shows the median of the angular separation $\Delta\theta$ of reconstructed bulk flow direction to the input values while the right panel shows its median uncertainty. [TODO: Leave out?]

$\sqrt{N}$. However, the left panel of Fig. 2 shows that the input velocity of 300 km s^{-1} is reconstructed better when adding southern SNe instead of northern ones. The simulations of only northern SNe converge at $\sim$ 250 km s^{-1}, showing the importance of correcting for a bias in the sky coverage. Similarly the angular separation of the reconstructed dipole direction and the input direction (Fig. 3) is smaller for a better sky coverage and continues to improve with larger statistics while it levels at $\sim 14^\circ$ for a purely northern survey.

The benefit of a full sky coverage becomes even more apparent when fitting the full tidal velocity field, i.e. including the shear term. The right panel of Fig. 4 shows the uncertainties of $v_{\rm d}$, which doubles for the simulations of only northern data but remains the same for full sky coverage. This be explained by the fact that the z–component of the velocity (in equatorial coordinates) and the shear component in the same direction cannot be constrained well at the same time if data on one hemisphere is missing, as can be seen by the following argument: both components can explain a velocity e.g. toward the north pole but differ in the dipole then predicts a velocity away from the south pole while the shear component predicts the velocities to be towards it [Is this argument clear to everyone?]. This can be seen as a large covariance between the fit results for these two components when fitting northern data, which is not present for full sky coverage. [TODO: Verify this. Need to transform covariance into equatorial system.] Similarly, the angular separation of best fit dipole direction and the input value (Fig. 5) increases compared to the dipole-only analysis.

Fig. 6 shows the shear components in eigenvector basis λ_i and their uncertainties. The eigenvalues are sorted in descending order, i.e. $\lambda_1 > \lambda_2 > \lambda_3$, and were calculated for the traceless shear tensor, i.e. $\lambda_2 = \lambda_3 = -\lambda_1/2$. The simulation input values were $\lambda_1 = 1.5$ km s^{-1} Mpc^{-1} and $\lambda_2 = \lambda_3 = -0.75$ km s^{-1} Mpc^{-1} with the first eigenvector aligned with the dipole. The results for the first eigenvalue λ_1 are not scattered around the true value but are consistently larger than the input, though still within the uncertainty. This can be explained by the sorting of the eigenvalues. Since λ_1 is always the largest eigenvalue, its distribution is

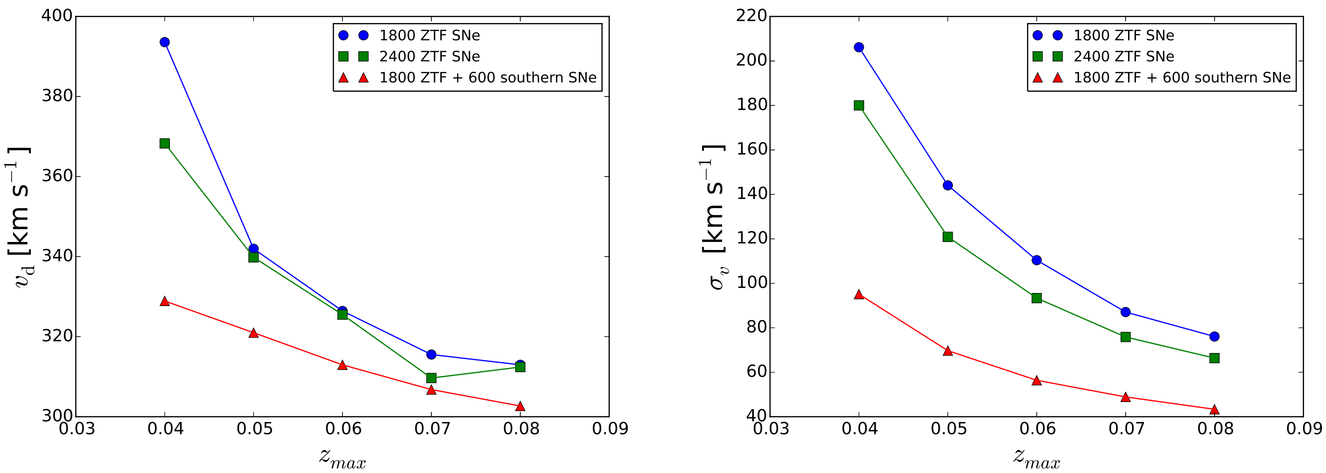

Fig. 4. Results for a tidal field fit to 1000 random realizations of the simulated data. The panels show the dipole velocity amplitude and uncertainty as in Fig. 2.

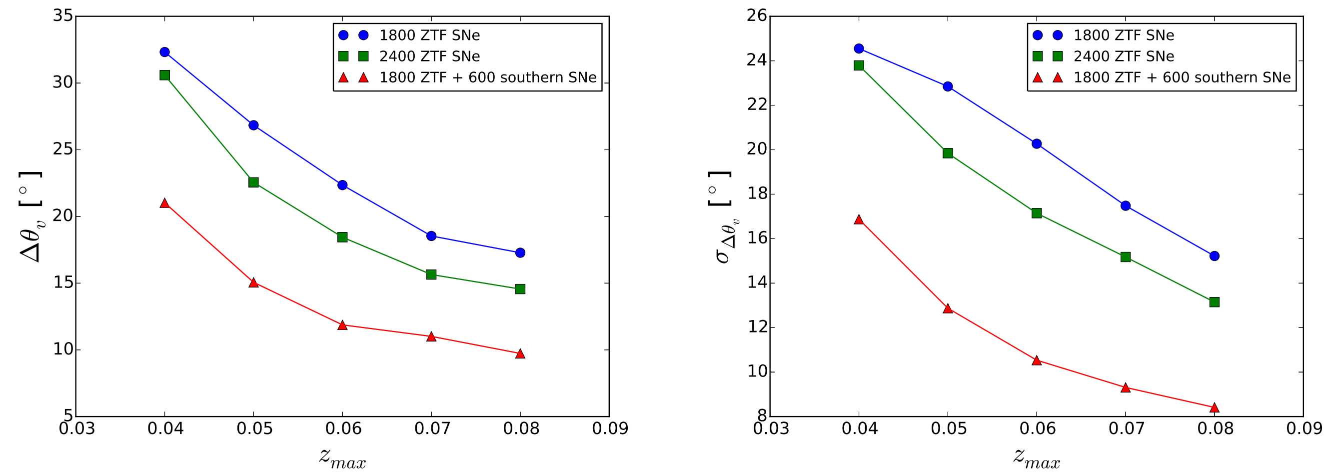

Fig. 5. Results for a tidal field fit as in Fig. 4. The panels show the deviation of the reconstructed direction from the input value as in Fig. 3. [Leave out? Or maybe only keep deviation without uncertainty?]

expected to be skewed towards values larger than the input. The other eigenvalues deviate to either side of the input value, with λ_2 being greater and λ_3 less than -0.75 km s^{-1} Mpc^{-1}. Again this is caused by the sorting of the eigenvalues, due to which the eigenvalues are limited to $\lambda_2 > -\lambda_1/2 > \lambda_3$. Therefore, the remaining deviation at $z_{max} = 0.08$ is only marginal.

The uncertainties shown in the right column of Fig. 6 are in fact the uncertainties of the diagonal terms of the shear matrix in the eigenvector basis.[3] For the smallest sphere ($z_{max} = 0.04$) the uncertainty is already at a similar level as the uncertainties of 0.7 km s^{-1} Mpc^{-1} to 1.0 km s^{-1} Mpc^{-1} found by Feldman et al. (2010). For large z_{max} the uncertainties decrease down to near 0.2 km s^{-1} Mpc^{-1}. Again adding southern data improves the results for 1800 northern SNe by a greater factor than norther data; the uncertainties decrease by 20–30 % instead of the 13 % expected from $\sqrt{N}$.

Fig. 7 shows the angular separations of the first eigenvector to the input direction (left panel) and the reconstructed bulk flow direction (right panel). For the former the full sky coverage is again finds the true value more reliably with a median separation that is about a third smaller than for the same number of northern SNe. This effect is not weaker for the angular separation to the reconstructed bulk flow direction but in all simulations it is still consistent with the uncertainties of the directions.

Fig. 8 shows the results for the monopole term of the tidal field. The consistently positive results for the monopole found for a northern survey are of interest beyond the study of velocity fields because the monopole term corresponds to a local change of the Hubble constant. Therefore, a large positive monopole could explain the tension between direct measurements of the Hubble constant using a distance ladder including SN Ia (e.g. Riess et al. 2011) and indirect measurements (e.g. using the CMB, Planck Collaboration XVI 2014). The monopole found here, however, is too small to be the sole explanation for the tension, and fully consistent with zero. For a full sky survey the median monopole decreases to less than half a percent of the Hubble constant for all redshitft ranges [TODO: Check that number, looks smaller than that.]. Therefore the monopole seen

[3] The actual uncertainties of the eigenvalues would be more difficult to calculate because they are solutions to a cubic equation.

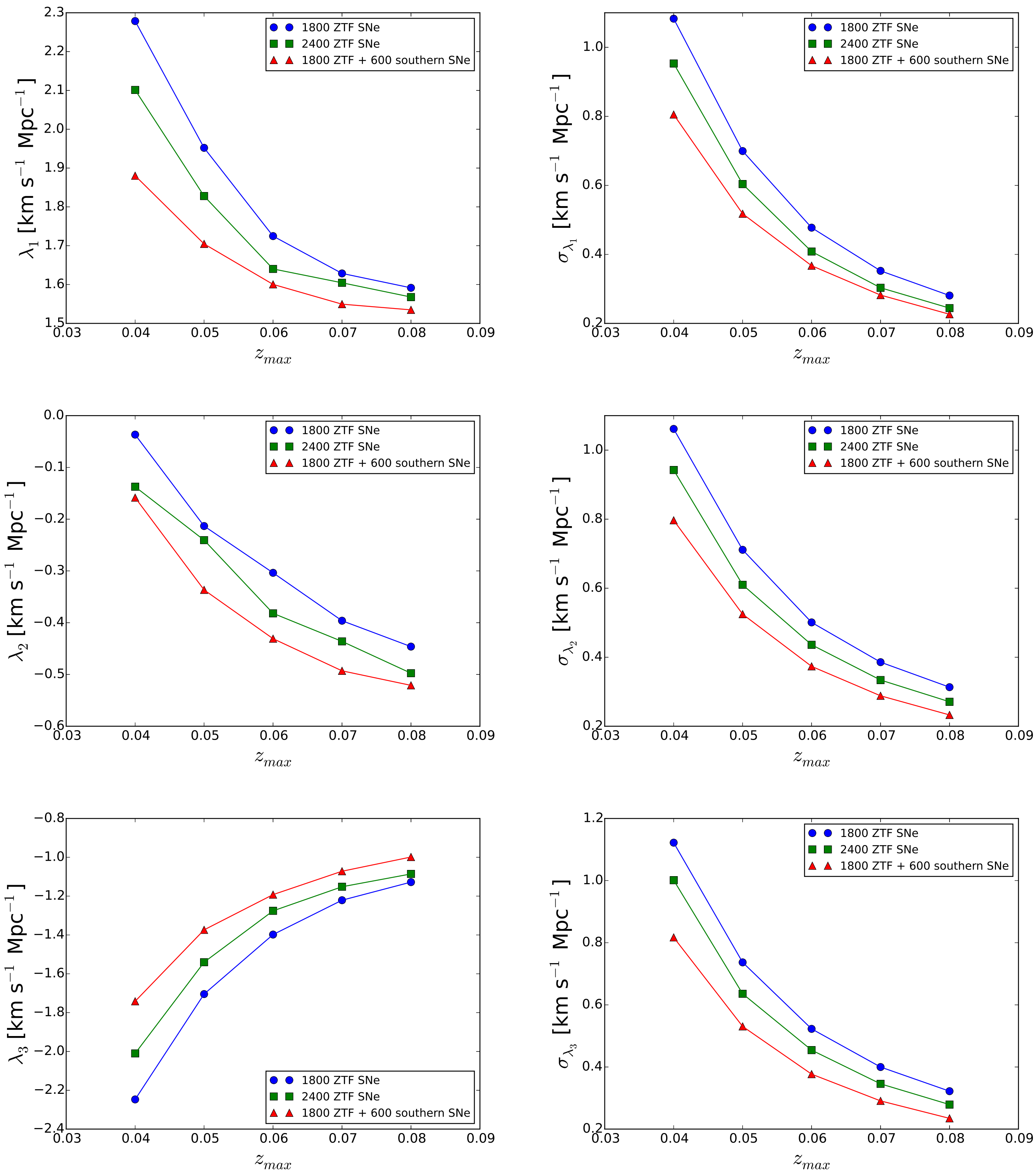

Fig. 6. Eigenvalues of the shear matrix and number of SNe simulations of a constant bulk and shear as in Fig. 4. The left column of panels shows the median eigenvalues Σ_i as a function of the upper redshift cut-off z_{max} while the right column shows the median of the uncertainties of the diagonal shear term in eigenvector basis.

for a northern survey appears to be only caused by the lack of sky coverage.

Fig. 9 shows a distance estimate R as defined by e.g. Kaiser (1991); Hoffman et al. (2001) as

$$R = \frac{2v_{\rm d}}{\tilde{\Sigma}}. \quad (6)$$

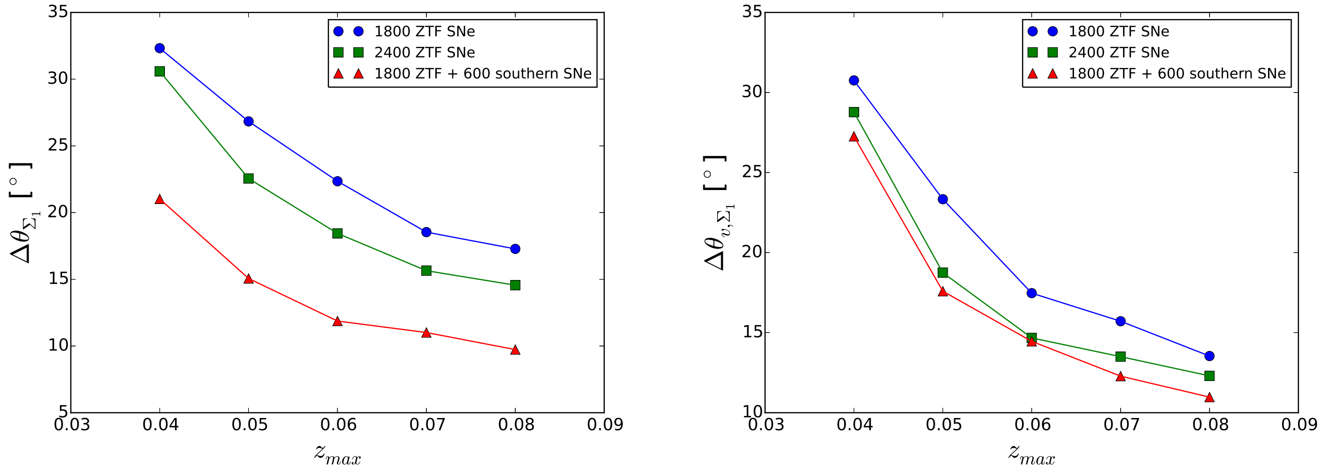

Fig. 7. Results for a tidal field fit as in Fig. 4. The panels show the median angular separation of the first eigenvector to the input direction and reconstructed bulk flow direction, respectively.

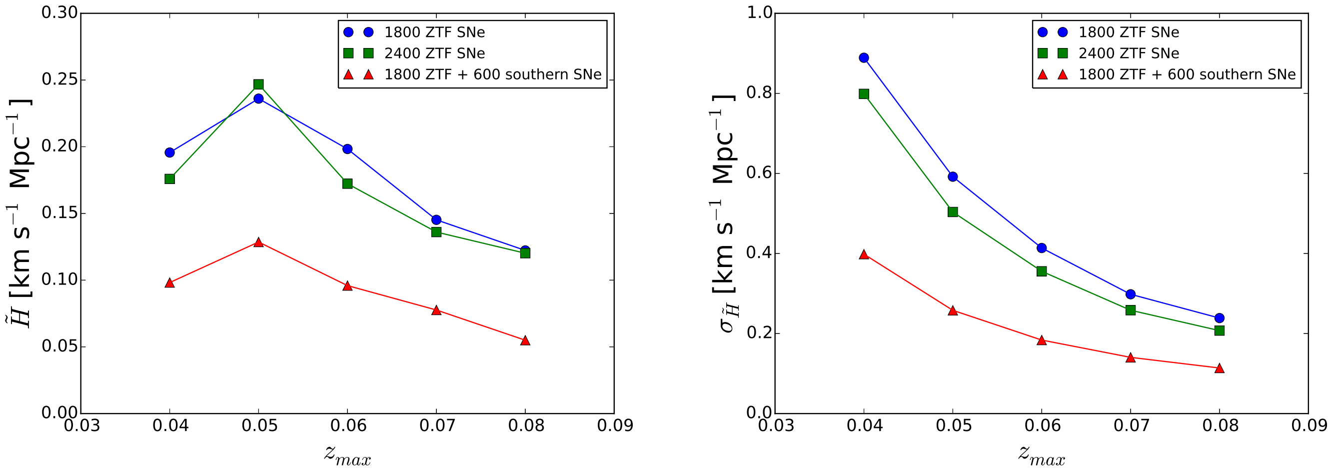

Fig. 8. Results for a tidal field fit as in Fig. 4. The upper left panel shows the median of the reconstructed monopole term $\tilde{H}$ as a function of the upper redshift cut-off z_{max} while the upper right panel shows its median uncertainty.

The simulation input corresponds to $R = 400\,\mathrm{Mpc}$, which is again not exactly found by the fit. Instead the distance is slightly overestimated, though still well within the uncertainties. This can be assumed to be an effect of the combined deviations of the dipole and shear measurements and, in case of the northern survey, the monopole term that does not fully vanish. The uncertainties appear to be decreasing monotonously but it should be noted that this is largely due to the stability of the shear over redshift. For a lower shear the uncertainty σ_R of the distance estimate will increase along with the distance estimate itself because it is defined by

$$\sigma_R^2 = \left(\frac{2\sigma_v}{\tilde{\Sigma}}\right)^2 + \left(\frac{2v_\mathrm{d}\sigma_{\tilde{\Sigma}}}{\tilde{\Sigma}^2}\right)^2 - \frac{8v_\mathrm{d}}{\tilde{\Sigma}^3}\mathrm{Cov}(v_\mathrm{d}, \tilde{\Sigma}). \quad (7)$$

For a more realistic attractor, the shear is expected to decrease with distance and thus the distance estimate will become less well constrained.

In conclusion, we find that the survey assumed in these simulations can constrain the combined dipole and shear out to $z = 0.08$ at a level that is up to two times better than the constraints found be Feldman et al. (2010) out to $z = 0.035$. Furthermore our results highlight that a survey of the northern sky like ZTF can gain greatly in constraining power when supplemented by a survey of the southern sky. Note that the data need not be restricted to SNe Ia but instead peculiar velocity data from galaxy surveys can serve the same purpose. [TODO: Add examples for such survey. Look up some details on 6dF. Also move (part of) this to conclusion section?]

4.2. Shell fits [working title]

[This could be left out as well if it makes the paper more readable but I like having a quick comparison of the shell fits as used in Feindt et al. (2013). If I leave it in I should maybe expand it a little.] As an additional analysis we fit the dipole model to the data binned in redshift shells, similar to the analysis preformed in Feindt et al. (2013). This method has the advantage that it can detect the changes in the dipole velocity that are expected for data behind a dominant attractor such as the Shapley supercluster. Using shells instead of spheres, however, decreases the

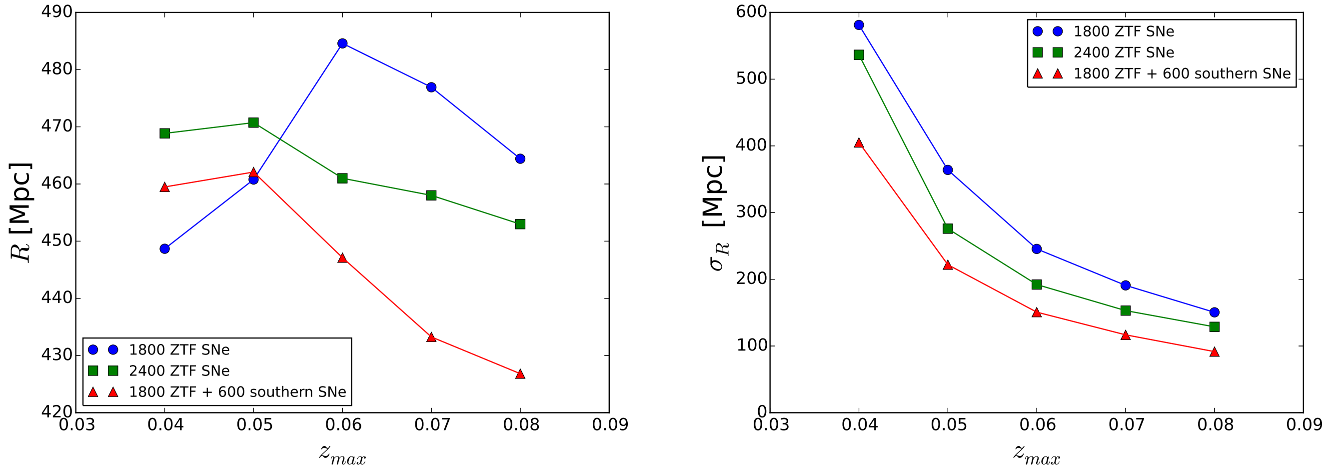

Fig. 9. Distance estimates and number of SNe per bin for simulations of a constant bulk flow and shear as in Fig. 4. The right panel shows the medians of the distance estimate $R = 2v_\mathrm{d}/\tilde{\Sigma}$ as a functions of the upper redshift cut-off z_{max} while the right panel shows its median uncertainty.

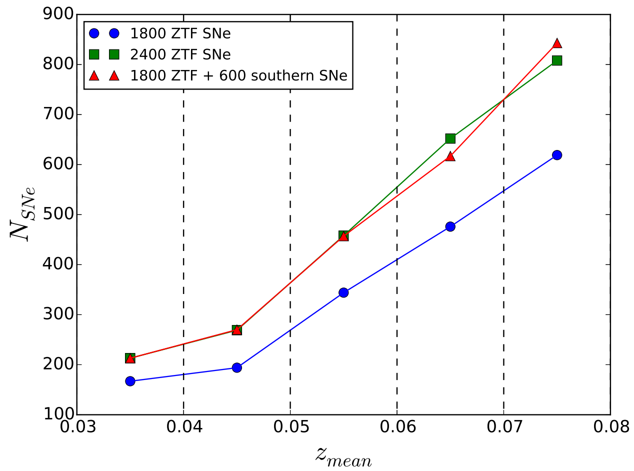

Fig. 10. Number of simulated SNe with redshift in redshift shells for simulations of 1800 and 2400 total SNe randomly drawn based on a constant volumetric supernova rate. The shell boundaries are shown as vertical dotted lines

number of SNe used in each bin. For this reasons we only fit the dipole model but not the full tidal velocity field. Fig. 10 shows the number of SNe per redshift shell.

The results for the dipole velocity amplitude (Fig. 11) are similar to those found for the sphere fits. The full-sky data reconstructs the input value of 300 km s^{-1} more accurately than northern data only. The uncertainties are ~ 300 km s^{-1} or lower for the simulations of 2400 SNe in all shells but show no significant difference based on sky coverage. This was also seen for the sphere fits when only fitting a dipole. Therefore, the uncertainties for northern surveys are expected to increase if we fit the shear as well. The direction of the bulk flow (Fig. 12) is reconstructed to within ~35° for the basic survey of 1800 SNe, adding 600 southern SNe reduces this to down almost 20°.

5. Conclusion

[TODO: Write.]

Acknowledgements. [TODO: add]

References

Bonvin, C., Durrer, R., & Kunz, M. 2006, Physical Review Letters, 96, 191302
Feindt, U., Kerschhaggl, M., Kowalski, M., et al. 2013, A&A, 560, A90
Feldman, H. A., Watkins, R., & Hudson, M. J. 2010, MNRAS, 407, 2328
Hoffman, Y., Eldar, A., Zaroubi, S., & Dekel, A. 2001, ArXiv Astrophysics e-prints [arXiv:astro-ph/0102190]
Kaiser, N. 1991, ApJ, 366, 388
Kashlinsky, A., Atrio-Barandela, F., Ebeling, H., Edge, A., & Kocevski, D. 2010, ApJ, 712, L81
Planck Collaboration XVI. 2014, A&A, 571, A16
Riess, A. G., Macri, L., Casertano, S., et al. 2011, ApJ, 730, 119

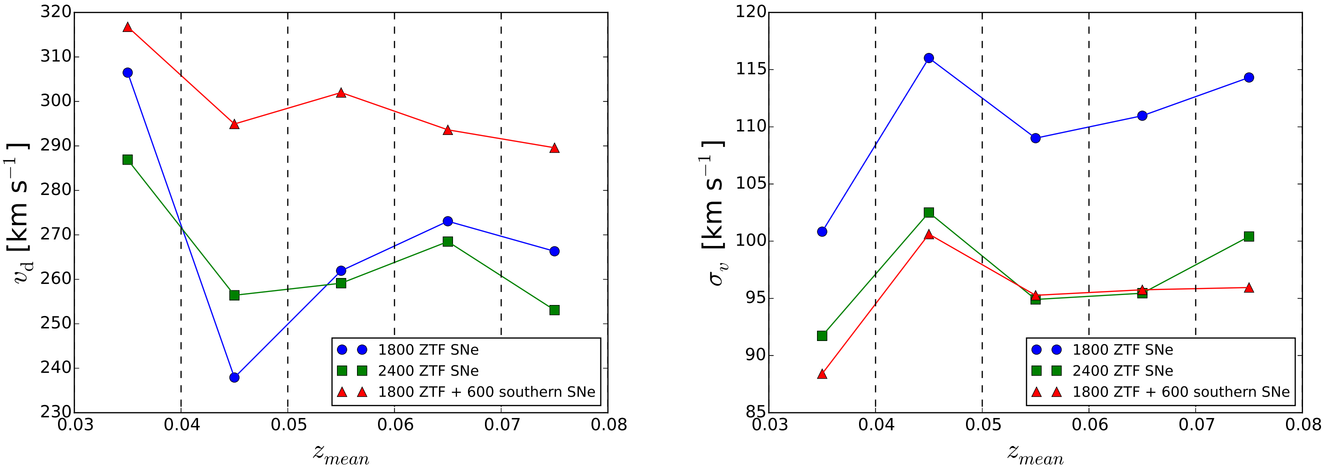

Fig. 11. Results for a bulk flow fit to 1000 random realizations of the simulated data. The left panel shows the median of the reconstructed dipole velocity amplitude v_d as a function of the mean redshift z_{mean} while the right panel shows its median uncertainty.

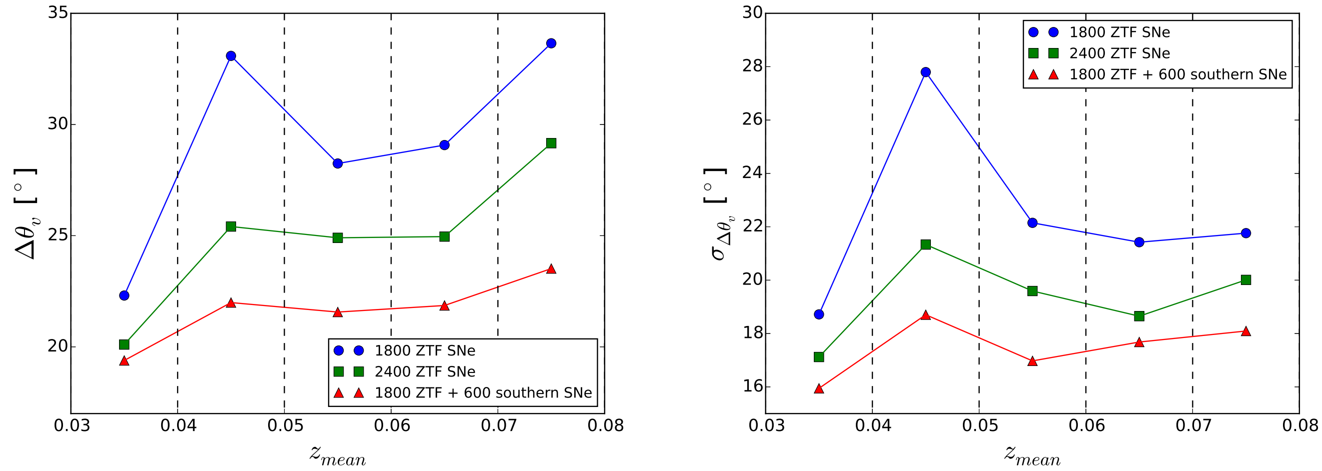

Fig. 12. Results for a bulk flow fit as in Fig. 11. The left panel shows the median of the angular separation $\Delta\theta$ of reconstructed bulk flow direction to the input values while the right panel shows its median uncertainty. [TODO: Leave out?]